# Ultrahigh 22 nm resolution coherent diffractive imaging using a desktop 13 nm high harmonic source

**Matthew D. Seaberg,[1,*] Daniel E. Adams,[1] Ethan L. Townsend,[1] Daisy A. Raymondson,[1] William F. Schlotter,[2] Yanwei Liu,[3] Carmen S. Menoni,[4] Lu Rong,[5] Chien-Chun Chen,[5] Jianwei Miao,[5] Henry C. Kapteyn,[1] and Margaret M. Murnane[1]**

[1]*JILA, University of Colorado, Boulder, Colorado 80309-0440, USA*
[2]*SLAC National Accelerator Laboratory, Menlo Park, California 94025, USA*
[3]*College of Engineering, University of California at Berkeley, California 94720, USA*
[4]*Department of ECE, Colorado State University, Fort Collins, Colorado 80523, USA*
[5]*Department of Physics and Astronomy and California NanoSystems Institute, University of California, Los Angeles, California 90095, USA*
**matthew.seaberg@colorado.edu*

**Abstract**: New diffractive imaging techniques using coherent x-ray beams have made possible nanometer-scale resolution imaging by replacing the optics in a microscope with an iterative phase retrieval algorithm. However, to date very high resolution imaging (< 40nm) was limited to large-scale synchrotron facilities. Here, we present a significant advance in image resolution and capabilities for desktop soft x-ray microscopes that will enable widespread applications in nanoscience and nanotechnology. Using 13nm high harmonic beams, we demonstrate a record 22nm spatial resolution for any tabletop x-ray microscope. Finally, we show that unique information about the sample can be obtained by extracting 3-D information at very high numerical apertures.



**OCIS codes**: (340.7460) X-ray microscopy; (100.5070) Phase retrieval; (340.7480) X-rays, soft x-rays, extreme ultraviolet (EUV); (190.2620) Harmonic generation and mixing.

## References and links

1. W. R. Zipfel, R. M. Williams, and W. W. Webb, "Nonlinear magic: multiphoton microscopy in the biosciences," Nat. Biotechnol. **21**(11), 1369–1377 (2003).
2. T. A. Klar, E. Engel, and S. W. Hell, "Breaking Abbe's diffraction resolution limit in fluorescence microscopy with stimulated emission depletion beams of various shapes," Phys. Rev. E Stat. Nonlin. Soft Matter Phys. **64**(6), 066613 (2001).
3. T. A. Klar, S. Jakobs, M. Dyba, A. Egner, and S. W. Hell, "Fluorescence microscopy with diffraction resolution barrier broken by stimulated emission," Proc. Natl. Acad. Sci. U.S.A. **97**(15), 8206–8210 (2000).
4. R. Henriques, C. Griffiths, E. Hesper Rego, and M. M. Mhlanga, "PALM and STORM: unlocking live-cell super-resolution," Biopolymers **95**(5), 322–331 (2011).
5. M. J. Rust, M. Bates, and X. Zhuang, "Sub-diffraction-limit imaging by stochastic optical reconstruction microscopy (STORM)," Nat. Methods **3**(10), 793–796 (2006).
6. J. Squier and M. Müller, "High resolution nonlinear microscopy: a review of sources and methods for achieving optimal imaging," Rev. Sci. Instrum. **72**(7), 2855 (2001).
7. J.-X. Cheng and X. S. Xie, "Coherent anti-Stokes Raman scattering microscopy: instrumentation, theory, and applications," J. Phys. Chem. B **108**(3), 827–840 (2004).
8. W. Chao, B. D. Harteneck, J. A. Liddle, E. H. Anderson, and D. T. Attwood, "Soft X-ray microscopy at a spatial resolution better than 15 nm," Nature **435**(7046), 1210–1213 (2005).
9. D. Y. Parkinson, G. McDermott, L. D. Etkin, M. A. Le Gros, and C. A. Larabell, "Quantitative 3-D imaging of eukaryotic cells using soft X-ray tomography," J. Struct. Biol. **162**(3), 380–386 (2008).
10. C. A. Larabell and M. A. Le Gros, "X-ray tomography generates 3-D reconstructions of the yeast, saccharomyces cerevisiae, at 60-nm resolution," Mol. Biol. Cell **15**(3), 957–962 (2003).
11. J. Nelson, X. Huang, J. Steinbrener, D. Shapiro, J. Kirz, S. Marchesini, A. M. Neiman, J. J. Turner, and C. Jacobsen, "High-resolution x-ray diffraction microscopy of specifically labeled yeast cells," Proc. Natl. Acad. Sci. U.S.A. **107**(16), 7235–7239 (2010).

#152373 - $15.00 USD Received 5 Aug 2011; revised 27 Aug 2011; accepted 28 Aug 2011; published 25 Oct 2011

12. J. Miao, P. Charalambous, J. Kirz, and D. Sayre, "Extending the methodology of X-ray crystallography to allow imaging of micrometre-sized non-crystalline specimens," Nature **400**(6742), 342–344 (1999).
13. B. Abbey, G. J. Williams, M. A. Pfeifer, J. N. Clark, C. T. Putkunz, A. Torrance, I. McNulty, T. M. Levin, A. G. Peele, and K. A. Nugent, "Quantitative coherent diffractive imaging of an integrated circuit at a spatial resolution of 20 nm," Appl. Phys. Lett. **93**(21), 214101 (2008).
14. B. Abbey, K. A. Nugent, G. J. Williams, J. N. Clark, A. G. Peele, M. A. Pfeifer, M. de Jonge, and I. McNulty, "Keyhole coherent diffractive imaging," Nat. Phys. **4**(5), 394–398 (2008).
15. C. Song, H. Jiang, A. Mancuso, B. Amirbekian, L. Peng, R. Sun, S. S. Shah, Z. H. Zhou, T. Ishikawa, and J. Miao, "Quantitative imaging of single, unstained viruses with coherent x rays," Phys. Rev. Lett. **101**(15), 158101 (2008).
16. S. Roy, D. Parks, K. A. Seu, R. Su, J. J. Turner, W. Chao, E. H. Anderson, S. Cabrini, and S. D. Kevan, "Lensless X-ray imaging in reflection geometry," Nat. Photonics **5**(4), 243–245 (2011).
17. M. Marvin Seibert, S. Boutet, M. Svenda, T. Ekeberg, F. R. N. C. Maia, M. J. Bogan, N. Tîmneanu, A. Barty, S. Hau-Riege, C. Caleman, M. Frank, H. Benner, J. Y. Lee, S. Marchesini, J. W. Shaevitz, D. A. Fletcher, S. Bajt, I. Andersson, H. N. Chapman, and J. Hajdu, "Femtosecond diffractive imaging of biological cells," J. Phys. At. Mol. Opt. Phys. **43**(19), 194015 (2010).
18. H. N. Chapman, A. Barty, M. J. Bogan, S. Boutet, M. Frank, S. P. Hau-Riege, S. Marchesini, B. W. Woods, S. Bajt, W. H. Benner, R. A. London, E. Plönjes, M. Kuhlmann, R. Treusch, S. Düsterer, T. Tschentscher, J. R. Schneider, E. Spiller, T. Möller, C. Bostedt, M. Hoener, D. A. Shapiro, K. O. Hodgson, D. van der Spoel, F. Burmeister, M. Bergh, C. Caleman, G. Huldt, M. M. Seibert, F. R. N. C. Maia, R. W. Lee, A. Szöke, N. Timneanu, and J. Hajdu, "Femtosecond diffractive imaging with a soft-X-ray free-electron laser," Nat. Phys. **2**(12), 839–843 (2006).
19. H. N. Chapman, A. Barty, S. Marchesini, A. Noy, S. P. Hau-Riege, C. Cui, M. R. Howells, R. Rosen, H. He, J. C. H. Spence, U. Weierstall, T. Beetz, C. Jacobsen, and D. Shapiro, "High-resolution ab initio three-dimensional x-ray diffraction microscopy," J. Opt. Soc. Am. A **23**(5), 1179–1200 (2006).
20. H. N. Chapman, S. Bajt, A. Barty, W. H. Benner, M. J. Bogan, S. Boutet, A. Cavalleri, S. Duesterer, M. Frank, J. Hajdu, S. P. Hau-Riege, B. Iwan, S. Marchesini, A. Sakdinawat, K. Sokolowski-Tinten, M. M. Seibert, N. Timneanu, R. Truesch, and B. W. Woods, "Coherent imaging at FLASH," J. Phys. Conf. Ser. **186**, 012051 (2009).
21. M. Bertilson, O. von Hofsten, U. Vogt, A. Holmberg, and H. M. Hertz, "High-resolution computed tomography with a compact soft x-ray microscope," Opt. Express **17**(13), 11057–11065 (2009).
22. M. Wieland, Ch. Spielmann, U. Kleineberg, T. Westerwalbesloh, U. Heinzmann, and T. Wilhein, "Toward time-resolved soft X-ray microscopy using pulsed fs-high-harmonic radiation," Ultramicroscopy **102**(2), 93–100 (2005).
23. F. Brizuela, Y. Wang, C. A. Brewer, F. Pedaci, W. Chao, E. H. Anderson, Y. Liu, K. A. Goldberg, P. Naulleau, P. Wachulak, M. C. Marconi, D. T. Attwood, J. J. Rocca, and C. S. Menoni, "Microscopy of extreme ultraviolet lithography masks with 13.2 nm tabletop laser illumination," Opt. Lett. **34**(3), 271–273 (2009).
24. G. Vaschenko, C. Brewer, F. Brizuela, Y. Wang, M. A. Larotonda, B. M. Luther, M. C. Marconi, J. J. Rocca, C. S. Menoni, E. H. Anderson, W. Chao, B. D. Harteneck, J. A. Liddle, Y. Liu, and D. T. Attwood, "Sub-38 nm resolution tabletop microscopy with 13 nm wavelength laser light," Opt. Lett. **31**(9), 1214–1216 (2006).
25. P. W. Wachulak, A. Bartnik, and H. Fiedorowicz, "Sub-70 nm resolution tabletop microscopy at 13.8 nm using a compact laser-plasma EUV source," Opt. Lett. **35**(14), 2337–2339 (2010).
26. R. L. Sandberg, D. A. Raymondson, C. La-O-Vorakiat, A. Paul, K. S. Raines, J. Miao, M. M. Murnane, H. C. Kapteyn, and W. F. Schlotter, "Tabletop soft-x-ray Fourier transform holography with 50 nm resolution," Opt. Lett. **34**(11), 1618–1620 (2009).
27. A. Ravasio, D. Gauthier, F. R. Maia, M. Billon, J.-P. Caumes, D. Garzella, M. Géléoc, O. Gobert, J.-F. Hergott, A.-M. Pena, H. Perez, B. Carré, E. Bourhis, J. Gierak, A. Madouri, D. Mailly, B. Schiedt, M. Fajardo, J. Gautier, P. Zeitoun, P. H. Bucksbaum, J. Hajdu, and H. Merdji, "Single-shot diffractive imaging with a table-top femtosecond soft x-ray laser-harmonics source," Phys. Rev. Lett. **103**(2), 028104 (2009).
28. K. S. Raines, S. Salha, R. L. Sandberg, H. Jiang, J. A. Rodríguez, B. P. Fahimian, H. C. Kapteyn, J. Du, and J. Miao, "Three-dimensional structure determination from a single view," Nature **463**(7278), 214–217 (2010).
29. X. Huang, H. Miao, J. Steinbrener, J. Nelson, D. Shapiro, A. Stewart, J. Turner, and C. Jacobsen, "Signal-to-noise and radiation exposure considerations in conventional and diffraction x-ray microscopy," Opt. Express **17**(16), 13541–13553 (2009).
30. X. Zhang, A. R. Libertun, A. Paul, E. Gagnon, S. Backus, I. P. Christov, M. M. Murnane, H. C. Kapteyn, R. A. Bartels, Y. Liu, and D. T. Attwood, "Highly coherent light at 13 nm generated by use of quasi-phase-matched high-harmonic generation," Opt. Lett. **29**(12), 1357–1359 (2004).
31. A. Rundquist, C. G. Durfee 3rd, Z. Chang, C. Herne, S. Backus, M. M. Murnane, and H. C. Kapteyn, "Phase-matched generation of coherent soft X-rays," Science **280**(5368), 1412–1415 (1998).
32. R. A. Bartels, A. Paul, H. Green, H. C. Kapteyn, M. M. Murnane, S. Backus, I. P. Christov, Y. Liu, D. Attwood, and C. Jacobsen, "Generation of spatially coherent light at extreme ultraviolet wavelengths," Science **297**(5580), 376–378 (2002).
33. Y. Nagata, Y. Nabekawa, and K. Midorikawa, "Development of high-throughput, high-damage-threshold beam separator for 13 nm high-order harmonics," Opt. Lett. **31**(9), 1316–1318 (2006).

#152373 - $15.00 USD Received 5 Aug 2011; revised 27 Aug 2011; accepted 28 Aug 2011; published 25 Oct 2011

34. R. W. Falcone and J. Bokor, "Dichroic beam splitter for extreme-ultraviolet and visible radiation," Opt. Lett. **8**(1), 21–23 (1983).
35. J. R. Fienup, "Reconstruction of an object from the modulus of its Fourier transform," Opt. Lett. **3**(1), 27–29 (1978).
36. V. Elser, "Random projections and the optimization of an algorithm for phase retrieval," J. Phys. Math. Gen. **36**(12), 2995–3007 (2003).
37. D. R. Luke, "Relaxed averaged alternating reflections for diffraction imaging," Inverse Probl. **21**(1), 37–50 (2005).
38. S. Marchesini, H. He, H. Chapman, S. Hau-Riege, A. Noy, M. R. Howells, U. Weierstall, and J. C. H. Spence, "X-ray image reconstruction from a diffraction pattern alone," Phys. Rev. B **68**(14), 140101 (2003).
39. M. Guizar-Sicairos, S. T. Thurman, and J. R. Fienup, "Efficient subpixel image registration algorithms," Opt. Lett. **33**(2), 156–158 (2008).
40. J. Steinbrener, J. Nelson, X. Huang, S. Marchesini, D. Shapiro, J. J. Turner, and C. Jacobsen, "Data preparation and evaluation techniques for x-ray diffraction microscopy," Opt. Express **18**(18), 18598–18614 (2010).
41. R. L. Sandberg, C. Song, P. W. Wachulak, D. A. Raymondson, A. Paul, B. Amirbekian, E. Lee, A. E. Sakdinawat, C. La-O-Vorakiat, M. C. Marconi, C. S. Menoni, M. M. Murnane, J. J. Rocca, H. C. Kapteyn, and J. Miao, "High numerical aperture tabletop soft x-ray diffraction microscopy with 70-nm resolution," Proc. Natl. Acad. Sci. U.S.A. **105**(1), 24–27 (2008).
42. B. Chen, R. Dilanian, S. Teichmann, B. Abbey, A. Peele, G. Williams, P. Hannaford, L. Van Dao, H. Quiney, and K. Nugent, "Multiple wavelength diffractive imaging," Phys. Rev. A **79**(2), 023809 (2009).
43. T. Popmintchev, M.-C. Chen, P. Arpin, M. M. Murnane, and H. C. Kapteyn, "The attosecond nonlinear optics of bright coherent X-ray generation," Nat. Photonics **4**(12), 822–832 (2010).
44. C. Wagner and N. Harned, "EUV lithography: lithography gets extreme," Nat. Photonics **4**(1), 24–26 (2010).

## 1. Introduction

The quest to understand structure, dynamics and function at the nanoscale continues to drive new ultrahigh-resolution imaging technologies. Electron microscopy is well established as a powerful method for obtaining images with sub-optical wavelength resolution, but cannot be applied to thick (i.e. >~100nm) samples, and suffers from a relatively low image contrast in most cases. Super-resolution optical imaging techniques such as multiphoton microscopy [1], stimulated emission depletion microscopy (STED) [2,3], photo-activated localization microscopy (PALM) and stochastic optical reconstruction microscopy (STORM) [4,5] have made impressive progress using visible light for super-resolution imaging. However, these techniques rely on scanning or on sparsely emitting labeled samples, where the centroid of single fluorescent molecules in the sample can be located down to 10 nm precision. Techniques that require labeling are useful when functional groups can be reliably and selectively labeled. However, this approach is invasive and requires considerable prior knowledge of the system. Powerful and widely-used label-free techniques such as multiphoton [6] or CARS microscopy [7] avoid these issues, but require scanning and yield only modestly-higher spatial resolution than conventional techniques such as confocal microscopy.

Soft x-ray microscopy is a general-purpose nanoscale imaging technique that complements electron and visible wavelength microscopies because it can penetrate thick samples (for 3-D imaging) and achieve very high spatial resolution with the added advantages of elemental and chemical specificity. To date, soft x-ray microscopy has been implemented primarily using light from synchrotron radiation facilities, with demonstrated spatial resolutions as high as 15 nm using zone plate based microscopes [8]. Soft x-ray microscopy has also proven to be uniquely capable of 3-D tomographic imaging of single cells with ~50 nm spatial resolution [9,10] and in 2-D with 11 nm resolution [11]. In exciting advances during the past decade, x-ray coherent diffractive imaging (XCDI) has emerged as a complementary approach to zone plate microscopy, provided that the illuminating beam is highly spatially coherent [12]. In XCDI, an object is illuminated with a coherent beam of light, and the light scattered from the object is then recorded using a CCD detector (see Fig. 1). An iterative phase retrieval algorithm can recover an image from the scattered-light diffraction pattern, essentially replacing the objective lens with a computer algorithm. XCDI has now been successfully implemented using a variety of coherent soft x-ray sources,

#152373 - $15.00 USD Received 5 Aug 2011; revised 27 Aug 2011; accepted 28 Aug 2011; published 25 Oct 2011

including synchrotrons [12–16], and x-ray free-electron lasers (XFELs) [17,18] in both single and multiple shot imaging modes. Using XCDI, the highest spatial resolution obtained to-date are 7 nm and 40 nm using synchrotron and XFEL sources, respectively [19,20].

However, despite the clear potential for x-ray microscopy to enable rapid advances in the nano- and bio-sciences, only a few of these microscopes exist worldwide, primarily because they can only productively be located at a small number of large synchrotron or x-ray free electron laser light sources. Although incoherent laser plasma-based soft x-ray sources can also be used for illuminating a zone-plate microscope, they have spatial resolutions limited by the zone plate and require exposure times on the order of several minutes [21]. Furthermore, for a host of scientific and technological grand challenges, there is a need for a widely available tool that can capture dynamics and structure with sub-10 nm spatial resolution and fs temporal resolution. These grand challenges include understanding how function is related to nanoscale inhomogeneities in catalytic, biological and energy-conversion systems, how heat dissipates in next-generation data storage devices, or how to design and characterize next generation integrated circuits in support of the relentless drive to shrink device dimensions.

Fortunately, in recent years rapid advances in compact coherent short wavelength light sources based on high harmonic generation and x-ray lasers have opened up new capabilities in tabletop soft x-ray microscopy. In past work, by using diffractive zone-plates as the objective and condenser in a conventional microscope configuration, record image resolutions of 38 nm were achieved using a 13 nm short-wavelength laser [21–25]. Other recent work using 30 nm wavelength high-harmonic beams (HHG) to implement soft x-ray coherent diffractive imaging achieved spatial resolutions of 50 nm with relatively long integration times of 80 minutes [26], and single shot imaging with 125 nm spatial resolution using longer wavelength harmonics [27].

Here, we present a significant advance in image resolution, data acquisition times and imaging capabilities for desktop soft x-ray microscopes that will enable widespread applications in nanoscience and nanotechnology. We demonstrate a new record spatial resolution of 22 nm for any compact light-based microscope using any light source or imaging methodology. Moreover, spatial resolutions of 25 nm can be obtained in only 30 seconds. Finally, we demonstrate 3-D reconstructed images made possible by collecting and deconvolving at high numerical apertures (NA) of 0.6 - 0.8 using ankylography [28]. This allows us to gain information about the sample not possible using other approaches. Our XCDI transmission microscope is driven by a 4W desktop femtosecond laser similar to that widely used in many laboratories worldwide. In the future, it will be straightforward to scale this microscope to sub-10 nm spatial resolution. In the case of reversible processes where stroboscopic accumulation of data is possible, the inherent temporal resolution of this XCDI high harmonic microscope is ~10 fs. Moreover, since single shot HHG imaging has already been demonstrated, the temporal resolution is limited only by the bandwidth that can be successfully deconvolved.

In the implementation of coherent diffractive imaging used for this work, the requirements for successfully recovering an image are: (1) illumination of the object with a coherent plane-wavefront with well-characterized and reasonably narrow spectral bandwidth; (2) isolation of the sample, where scattered light all originates only from the object region; and (3) oversampling of the scattered light, where the diffracted light pattern must be recorded with sufficient resolution to remove the ambiguity introduced by the fact that the CCD detector only records an intensity pattern, and loses the optical phase information required for simple Fourier transform reconstruction of an image. If these requirements are met, XCDI has several significant advantages over conventional microscopy. First and foremost, the obtainable image resolution is no longer limited by the optics. This is in contrast to zone plate imaging, where the spatial resolution is limited by the width of the outermost-zone that can be fabricated, fundamentally limiting this technique to the resolution of current nano-fabrication capabilities. Second, XCDI is more photon-efficient, since all scattered photons from the

#152373 - $15.00 USD Received 5 Aug 2011; revised 27 Aug 2011; accepted 28 Aug 2011; published 25 Oct 2011

sample are detected [29]. This reduces both source flux requirements and radiation exposure to the sample. However, the drawbacks of XCDI include the requirement for a coherent illumination source, and need for a computer deconvolution to obtain an accurate image. These disadvantages have been convincingly addressed over the past decade, by faster algorithms and computers, higher flux coherent soft x-ray light sources based on x-ray free electron lasers and high harmonic sources, and a wide range of successful image retrievals.

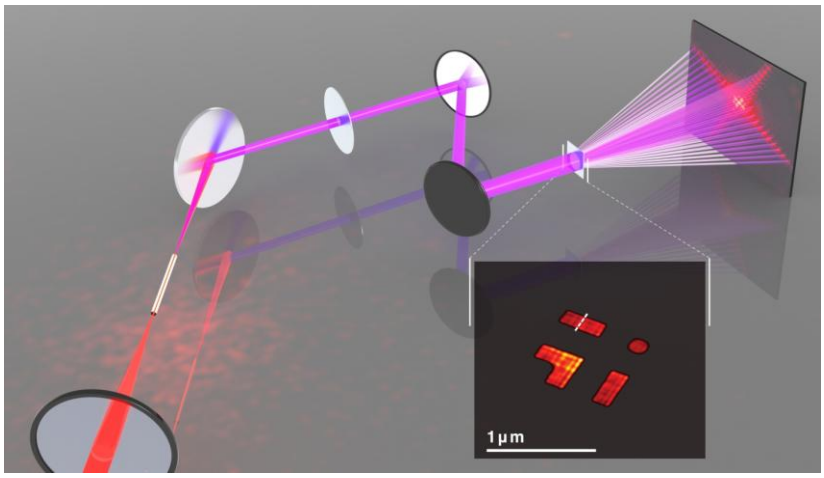


Fig. 1. Experimental configuration for tabletop soft x-ray coherent diffractive imaging. A femtosecond laser is focused into a gas-filled waveguide. Bright, coherent 13 nm high harmonic beams are produced and focused into the sample. The resultant diffraction pattern is captured on a CCD camera and the image is retrieved using an iterative phase retrieval algorithm.

## 2. Methods

Figure 1 shows a schematic of the tabletop high harmonic generation (HHG) source and microscope used in this work. Light from an ultrafast Ti:sapphire laser-amplifier system (KMLabs Dragon , 2 mJ pulse energy, 780 nm wavelength, 2 kHz repetition rate, 25 fs pulse duration) is focused into a 5 cm long, 150 μm diameter, helium-filled hollow waveguide to generate fully coherent high-harmonic beams around 13 nm [30]. An increased high harmonic flux at 13 nm was critical to our experiments, in order to significantly enhance the spatial resolution with much reduced exposure times. The waveguide geometry allows a long interaction length to establish excellent laser and HHG modes that can be fully phase matched and fully spatially coherent [30–32]. Moreover, at 13 nm wavelength, the nonlinear medium (He) is strongly absorbing, and the gas pressures required for phase matching are very high (≈1 atm). Unless the high harmonic beam emerges into vacuum over a sharp gas density gradient, the losses due to phase mismatch in the end sections and gas absorption can be significant.

To reject the laser light that co-propagates with the high harmonic beam, we use a combination of a Brewster-angle silicon substrate coated with ~210 nm of $ZrO_2$ [33,34], combined with two 200 nm thick Zr filters. The Brewster plate absorbs nearly all of the infrared light and reflects ~60% of the HHG beam, while the filters each have a calculated transmission of 50% at 13 nm. The broadband EUV light is then spectrally filtered and refocused onto the sample using a pair of 73% efficient multilayer reflectors centered at 12.8 nm (1 flat and one 1 m ROC), resulting in a flux of $>10^8$ photons/s *at the sample*. After illuminating the sample, the scattered light is collected in the far field using a back-illuminated, x-ray sensitive CCD detector with 13.5 micron square pixels on a 2048x2048 array (Andor iKon DO436). In the far field, the diffraction pattern is related to the exit wave of the object by a Fourier transform. Using the Hybrid Input-Output (HIO) phase retrieval

#152373 - $15.00 USD Received 5 Aug 2011; revised 27 Aug 2011; accepted 28 Aug 2011; published 25 Oct 2011

algorithm [35], it is possible to recover the phase information and consequently an image of the object.

Two different test objects were used to test the spatial resolution of our XCDI desktop microscope, shown in SEM images in Fig. 2(a) and 2(e) (referenced hereafter as J407 and J409). Raw diffraction data are shown in Fig. 2(c) and 2(g), while reconstructions are shown in Fig. 2(b) and 2(f). Before reconstructing the image, the raw data must be preprocessed to improve the convergence of the iterative algorithm. First, hot pixels inherent to the CCD chip are removed, and cosmic rays appearing in the final scatter pattern are identified and removed. In some cases, filtering was performed in the Fourier space of the scatter pattern. Finally, the full diffraction pattern was binned by a factor of eight for sample J407 and sixteen for sample J409. The binning process combines photon counts from adjacent pixels into a single pixel, increasing signal to noise and decreasing the overall grid size for the calculation.

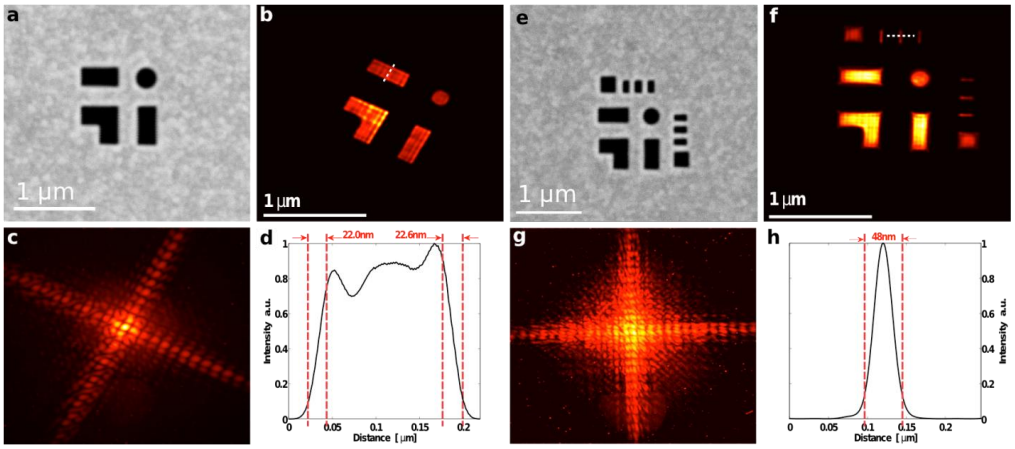


Fig. 2. Sub-25nm resolution confirmed using a knife-edge test. (a), (e) Scanning electron microscope images of samples J409 and J407 respectively. (b), (f) Object intensities reconstructed using the HIO algorithm. (c), (g) Scatter patterns for objects J409 and J407 respectively. (d) Lineout showing an edge with a ~22nm 10% to 90% dimension. (h) Object J407 displays minimum feature sizes of ~50nm ($e^{-2}$ diameter) providing a rough estimate of resolution. The lineouts in (d) and (h) were taken along profiles marked in (b) and (f) by white dashed lines.

After the data was filtered, several well-established iterative phase retrieval algorithms were implemented to reconstruct the amplitude and phase of the images, including difference map [36], HIO [35] and RAAR [37]. All of these algorithms converged to the same final object amplitudes. For the results shown in Fig. 2, we used the HIO algorithm, replacing the diffraction amplitude with experimental data after each iteration to serve as as the Fourier-domain constraint, and a shrinking support [38] as the object-space constraint. The details of the full iterative algorithm are as follows: the HIO algorithm was allowed to converge, after which 1000 final iterations were averaged together to form one independent reconstruction. Thirty such fully independent reconstructions were averaged together to form the solution. Because independent solutions to the phase retrieval are equivalent except for the center positions of the image, independent reconstructions must first be registered with one another using sub-pixel cross-correlation and then interpolation [39].

## 3. Results and discussion

The data for object J407 (Fig. 2(e)–2(h)) were obtained with the CCD placed 3.6 cm past the object, corresponding to a NA of ~0.36. This allows for a maximum half-pitch resolution using coherent illumination of $\Delta r_{hp} = 0.5\ \lambda/NA \approx 18$nm, calculated using the Rayleigh criterion for coherent illumination. The lineout shown in Fig. 2(h) was taken along the profile marked

#152373 - $15.00 USD Received 5 Aug 2011; revised 27 Aug 2011; accepted 28 Aug 2011; published 25 Oct 2011

in Fig. 2(f) by a dashed, white line. The $e^{-2}$ diameter of this nano-fabricated feature is ~50 nm, which provides an upper limit for our imaging resolution. Object J409 (Fig. 2(a)–2(d)) was placed 4.6cm from the CCD, corresponding to a NA ~0.28. Using NA = 0.28 the half-pitch resolution would be $\Delta r_{hp} \approx 23$nm. However, Fig. 2(b) clearly shows a strong signal to noise ratio out to the corner of the CCD which increases the NA to 0.4, giving an angle-dependent Rayleigh criterion resolution between 17nm and 23nm. The Rayleigh criterion states the maximum resolution of an imaging system, $\Delta r_{hp}$, as the ability to resolve two points spaced by 2 x $\Delta r_{hp}$. In our case however, the sample simply does not contain features this small (the smallest feature is ≈50 nm). A conventional alternative to the Rayleigh criterion is to test the distance over which an edge makes a transition from dark to light by measuring the distance between 10% and 90% of the maximum sample intensity. This method is known as the knife-edge test, and the results of such a test are shown in Fig. 2(d). Both edges in Fig. 2(d) transition from dark to light in a distance ~22nm, in excellent agreement with the resolution expected based on the NA used for this image. We note that the half-pitch resolution calculated using the Rayleigh criterion is usually directly associated with the distance measured using the knife-edge test. However, we point out that the relationship between resolutions measured using the knife-edge test and the Rayleigh criterion is actually closer to $\Delta r_{KE} \approx 85\% \Delta r_{RC}$, yielding a resolution of 23 nm, in excellent agreement with our data.

After reconstructing the object from its scatter pattern, the pixel size was decreased by a factor of 16 in the images plotted in Fig. 2(b), 2(f) in order to accurately ascertain the 10% and 90% points of the intensity across an edge. The pixel size was modified via Fourier transform, zero-padding interpolation. Even though the pixel sizes in Fig. 2(b), 2(f) were significantly decreased, no information was added because both objects were originally sampled at a frequency greater than the Nyquist frequency.

While the knife-edge test is convenient and provides an accurate resolution measure of an edge transition, a somewhat more powerful tool is the phase-retrieval transfer-function (PRTF), defined as

$$PRTF(f) = \sum_{f=const} \varphi(f). \tag{1}$$

The diffraction phases $\phi(f)$ are averaged over constant frequency contours to produce the PRTF, which takes a value of 1 where the iterative algorithm produced perfect convergence consistently, and a value near 0 where the algorithm continually failed to converge. Before using Eq. (1) as a measure of the reconstructed image resolution, we constructed a Weiner filter [40] of the form

$$W(f) = \frac{|S(f)|^2}{|S(f)|^2 + |N(f)|^2} \tag{2}$$

where S($f$) is the power spectral density of the measured diffraction pattern and N($f$) is a measure of the noise trend, taken to be a constant 0<N<1 for our filter. We implemented the Weiner filter to produce an improved measure of image quality as WPRTF($f$) = W($f$)PRTF($f$), which is shown in Fig. 3.

#152373 - $15.00 USD Received 5 Aug 2011; revised 27 Aug 2011; accepted 28 Aug 2011; published 25 Oct 2011

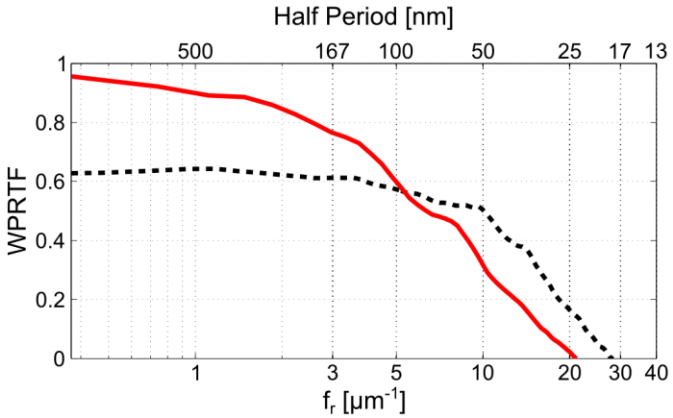


Fig. 3. Filtered phase-retrieval transfer-function. Features in the WPRTF provide a measure of the smallest sample features and the image resolution of reconstructed images. For example, the WPRTF for sample J407 shows a "knee" structure around 50nm half-period resolution, which corresponds to the feature size of the slots of ~50nm. The cutoff WPRTF values are between 19 and 22nm, in excellent agreement with the knife-edge measurements shown in Fig. 2.

Two critical features in the WPRTF can be used to express different types of image resolution. The WPRTF displays a "knee" type structure where the slope increases rapidly in the negative direction. The point where the slope changes is interpreted as the minimum feature size in the sample. This is evident for sample J407, where the minimum sample feature size from the SEM image and our retrievals is ~50nm, in excellent agreement with the position of the "knee" in the WPRTF. The second feature is the cutoff value of the WPRTF, which can be interpreted as the maximum resolution achieved in the reconstruction. The cutoff value for sample J407 displays a maximum resolution of ~19nm, while the cutoff value for sample J409 indicates a maximum resolution of ~22nm, in excellent agreement with the knife-edge measurement and NA of the imaging system. Non-uniform illumination accounts for the variation in brightness over the reconstructed image, because the 13 nm beam was focused at the sample to a spot size not much larger than the sample itself.

While independent reconstructions may only take ~1 min on a standard personal computer, the limiting factor for near real-time imaging using tabletop high harmonic x-ray sources is the limited amount of available photon flux. By increasing the x-ray flux *at the sample* to a value of $>10^8$photons/s, Fig. 4 displays sample J409 reconstructed after on-chip binning (performed by the Andor camera) to a grid size of 256x256 pixels using significantly shorter exposure times. The knife-edge test demonstrates a spatial resolution of ~25 nm in an image acquisition time of only 30 seconds.

Since in our initial experiments the diffraction patterns (Fig. 2(c), 2(g)) clearly extended beyond the edges of the CCD chip, we shortened the sample-to-CCD distance to just over 10 mm, corresponding to a NA = 0.79. It is well known from diffraction tomography that when collecting a pattern at such large angles, the 2-D pattern can actually be mapped onto a spherical shell of radius $1/\lambda$ in the 3-D Fourier transform space, termed the Ewald sphere. It is important to note that for a thick sample (relative to the 2-D projection of the object in the direction of illumination) in combination with diffraction collection at a high NA, there is modulation in the pattern due to the depth information encoded in the 3-D pattern. In this case, the curvature correction described in previous work [41] does not recover the intensity of the 2-D Fourier transform of the object. To accurately recover the object to the resolution corresponding to the NA, a 3-D reconstruction technique – such as ankylography or tomography - must be employed.

#152373 - $15.00 USD Received 5 Aug 2011; revised 27 Aug 2011; accepted 28 Aug 2011; published 25 Oct 2011

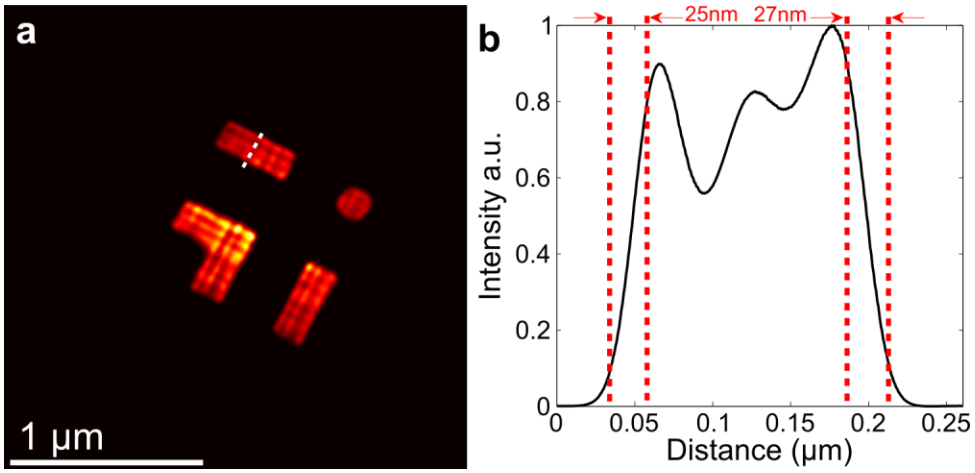


Fig. 4. Sub-30nm resolution from a 30 second exposure. Increases in HHG flux enabled by better differential pumping have led to a dramatic decrease in required exposure times. This has enabled 25 nm spatial resolution in an image with only 30 second exposure time.

In the 0.79-NA geometry, the diffraction pattern was above the noise level out to an angle corresponding to ~0.6 NA. This data was mapped onto the Ewald sphere as described in Raines et al. [28] and the result is shown in Fig. 5(a). In this case the spherical shell is positioned in a 3-D cube, and the points in the cube where data is absent must be retrieved in addition to the phase at the known intensity points. The 0.6 NA imaging allows a best possible resolution $\Delta r_{hp}$ of 10 nm in the x and y dimensions and 32 nm in the z dimension. An isosurface rendering of the resulting 3-D reconstruction is shown in Fig. 5(b), while a movie of the 3-D reconstruction is shown in Media 1. Since the walls of the sample are very absorbing at 13 nm, not all x-rays initially scattered reach the detector. Thus, this particular sample is not ideal for 3-D image reconstruction. Nevertheless, we are able to see that the sample was tilted by ~10 degrees with respect to the detector (Fig. 5(c)) and also extract the relative size difference between features in the sample. This is interesting because the sample was fabricated on a 50-100 nm thick silicon nitride membrane. Thus, the scanning electron microscope images shown in Fig. 2(a), 2(e) can only be taken from the front side, where the different etch depths are not apparent. In the future, the robustness of this high-NA 3-D imaging may be improved by illuminating an object with a broad bandwidth (e.g. several adjacent harmonics), thus filling in a significantly larger portion of the cube, using an extension of the technique demonstrated in Chen et al. [42]

## 3. Conclusion

In conclusion, we have significantly advanced imaging resolution for desktop-size soft x-ray microscopes by demonstrating a new record spatial resolution of 22 nm. By increasing the 13 nm high harmonic flux by 10– 100x, image resolutions of 25 nm can be obtained in only 30 sec. Moreover, we can extract information about the etch depth in the sample that cannot be obtained using electron microscopy. Advances in bright high harmonic sources at even shorter 1 nm wavelengths [43] will allow high contrast, elemental and chemical specific nano and bio imaging. Moreover, since EUV lithography will use light at 13 nm, and first-generation EUV lithography is expected to produce feature sizes of 22nm, the demonstrated resolution is capable of providing detailed image information on EUV lithographic masks or nano bit patterned data storage media [44]. Finally, dynamic imaging with unprecedented combined spatial (< 10 nm) and temporal resolution (< 10 fs) will be possible in the future.

#152373 - $15.00 USD Received 5 Aug 2011; revised 27 Aug 2011; accepted 28 Aug 2011; published 25 Oct 2011

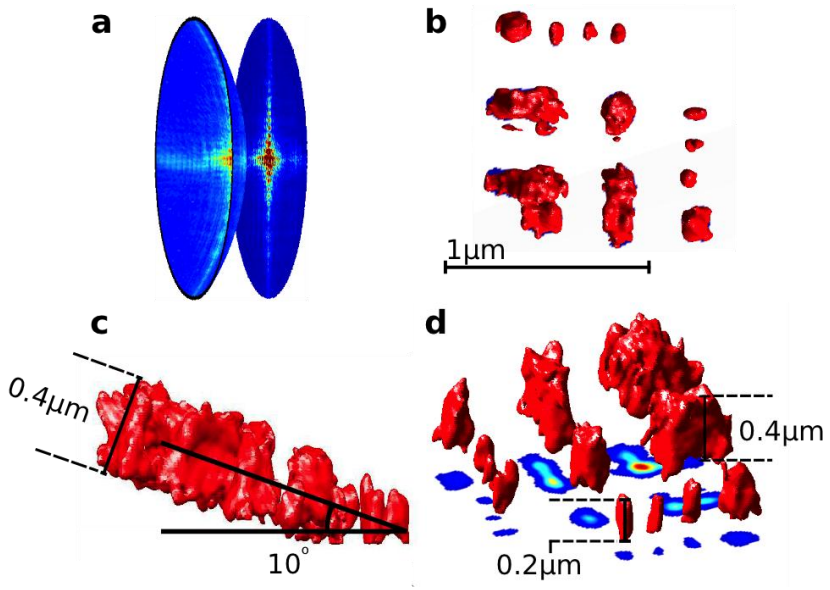


Fig. 5. (Media 1) Demonstration of ankylography with a high-NA diffraction pattern. (a) Diffraction pattern mapped onto the surface of the Ewald sphere accompanied by a projection onto the plane. (b**)** Isosurface rendering of the 3-D ankylographic reconstruction. (c) Same as in (b) showing tilt of sample with respect to the detector. (d) Same as in (b) showing the relative size difference between features in the sample with emphasis in the z-direction, accompanied by a projection onto the plane.

**Acknowledgments**

The authors acknowledge support from the DOE NNSA, NSSEFF, and the National Science Foundation Engineering Research Center in EUV Science and Technology. M. S. acknowledges support from the NSF IGERT program.

#152373 - $15.00 USD Received 5 Aug 2011; revised 27 Aug 2011; accepted 28 Aug 2011; published 25 Oct 2011